

## High pressure superconducting phase diagram of ${}^6\text{Li}$ : anomalous isotope effects in dense lithium

Anne Marie J. Schaeffer, Scott R. Temple, Jasmine K. Bishop and Shanti Deemyad

*Department of Physics and Astronomy, University of Utah, Salt Lake City, Utah, 84112*

Abstract: We report the superconducting transition temperature of  ${}^6\text{Li}$  between 16-26 GPa, the lightest system to exhibit superconductivity to date. The superconducting phase diagram of  ${}^6\text{Li}$  is compared to that of  ${}^7\text{Li}$  through simultaneous measurement in a diamond anvil cell (DAC)<sup>1,2</sup>. Below 21.5 GPa, Li exhibits a direct, but unusually large isotope effect, while between 21.5-26 GPa, lithium shows an inverse superconducting isotope effect. The unusual dependence of the superconducting phase diagram of lithium on its atomic mass provides evidence that quantum solid effects dominate the low temperature properties of dense lithium leading to anomalous differences in the structures and/or in electronic properties of the isotopes through zero point effects.

In a quantum solid, a large zero-point displacement of ions from lattice sites, comparable to inter-atomic distance, exists. Therefore the properties of a quantum solid do not adhere to static lattice models. The emergence of exotic quantum states in a compressed light metallic system has been entertained theoretically for metallic phases of hydrogen (e.g.<sup>3,4</sup>). Metallic hydrogen is predicted to have a liquid ground state, and may exhibit a two component superfluid and superconducting phase<sup>4,8</sup>. The difficulty of compressing hydrogen to densities sufficient for metallization, however, has prevented experimental proof of these effects<sup>9</sup>. Studying the properties of lithium, which is isovalent to hydrogen, is an alternative route to studying the evolution of lattice quantum effects in a dense light metallic system<sup>10</sup>. In systems with short range interactions, such as noble-gas solids, the lattice becomes more classical under compression<sup>11</sup>. By contrast, in systems that have long range interactions, such as metals, the ratio of lattice zero-point displacements to interatomic distances may increase under compression, provided they retain their long range interactions<sup>12</sup>. In these systems, more quantum solid behavior is expected at higher densities. As the only monovalent metal which exhibits superconductivity at one atmosphere, lithium has a notable position on the periodic table<sup>13-17</sup>. The significance of lattice quantum dynamics in lithium, even at ambient pressure, is evident from its temperature driven martensitic transition from bcc to hR9. At sufficiently low temperatures, where thermal energy plays a less dominant role in lattice dynamics, observation of lattice quantum dynamics is possible by studying properties of stable lithium isotopes, which have ~17% mass difference. Sound velocity measurements on stable isotopes of lithium at 77 K and less than 1.6 GPa show that quantum solid effects in lithium, at least in the pressure range studied, do not decrease as a function of pressure<sup>18</sup>. Raman spectroscopy studies between 40-

123 GPa and at 177 K report a reduced isotope effect in high frequency vibrational modes of Li, which may be related to quantum solid behavior<sup>19</sup>. Up to this point, no experiments have reported a comparison of any physical properties of lithium isotopes at low temperatures and high pressures concurrently. Since the superconducting transition of lithium occurs in a relatively low temperature range<sup>20-22</sup>, studying its superconducting isotope effect provides excellent conditions to search for quantum lattice effects and their evolution as a function of pressure.

In the present study, we have measured the superconducting isotope effects in the stable isotopes of lithium under pressure. Lithium is a simple metallic system which is expected to exhibit conventional phonon mediated superconductivity and a well defined superconducting isotope effect with nominal pressure dependence<sup>23</sup>. Since phonon-mediated superconductivity depends on lattice and electronic properties of a material, any unusual isotopic mass dependence of the superconducting phase diagram will provide evidence of possible quantum solid effects on electronic and/or structural properties.

For a BCS-type superconductor composed of one atomic species, with a static lattice, the superconducting transition temperature ( $T_c$ ) and the ionic mass follow the simplified relationship,  $T_c \propto M^{-\alpha}$ , in which  $\alpha=0.5$ . This relation is mainly attributable to differences in the Debye temperature for different ionic masses of different isotopes. In a non-static lattice and in the presence of large quantum zero point motion of ions, electrons do not see the lattice as a perfect crystal (this is the case even if these displacements do not affect the structures of the isotopes). On the first order, one expects a suppression of effective electron-ion interaction. This is a quantum analogy of Debye-Waller effects: non-static lattice effects caused by thermal energy. Debye-Waller factors, which are clearly functions of mass, will enter the band-structure; thus, in total, drastic deviations from conventional isotope effects in a superconducting quantum solid can be expected<sup>24, 25</sup>.

In addition to the electronic effects mentioned above, quantum solids may have structural differences between isotopic species. In a classical solid and in the absence of large zero point energy, the equilibrium distance between the lattice particles is determined by the minimum of the potential energy of the lattice and, to first approximation, is independent of the particles' mass<sup>26, 27</sup>. Therefore, in a classical solid, isotope effects in the structures are not expected. On the other hand, in a quantum solid, the large zero point energy of the lattice will significantly contribute to the vibrational and rotational energies, which can have an impact on the equilibrium structures<sup>26, 27</sup>. Since BCS assumes identical structures for isotopes, the BCS superconducting isotope relation is not applicable in systems with a structural isotope effect.

The expected conventional isotopic change in  $T_c$  of lithium is  $T_c^6 \approx 1.08T_c^7$ , which leads to a relatively small temperature shift at low temperatures, where lithium becomes a superconductor ( $T_c^7(\text{max}) \leq 20\text{K}$ , for which a BCS isotope shift of +1.6 K is expected for  ${}^6\text{Li}$ )<sup>20-22</sup>. This small difference in the relative  $T_c$ 's and lack of *in situ* thermometry in a DAC make conducting experiments sensitive enough to resolve the differences challenging. Only highly accurate temperature and pressure determination methods allow resolution of these isotopic differences. If there is any inconsistency in the temperature measurement between experimental runs, the expected isotope effect could easily be lost. In addition to experimental uncertainties, differences in a sample's thermal history may change  $T_c$ <sup>28</sup>. This is especially so for Li, in which the boundaries of the martensitic transition can be shifted if the sample is not annealed<sup>29</sup>. To achieve the required resolution in evaluating the relative  $T_c$ 's of the two samples, both isotopes were measured simultaneously inside the same DAC. The details of these experiments are given below, and the general principles of the method used have been previously published<sup>1</sup> (fig. 1). Previous comparative measurements on the low temperature electrical resistivity of lithium isotopes under ambient pressure also noted the importance of simultaneous measurements; however, simultaneous electrical measurements on large samples under ambient pressure are far less technically limiting than similar measurements under high pressure<sup>28</sup>. Similar considerations regarding the thermal history would be important for any comparative studies, such as structural or magnetic studies on lithium isotopes. In the present work, we have used two isotopically rich samples of lithium; a  ${}^6\text{Li}$ -rich sample (the  ${}^6\text{Li}$  samples contained 99.99% lithium with the isotopic composition 95.6%  ${}^6\text{Li}$  and 4.4%  ${}^7\text{Li}$  together with the impurities Na, Mg, Al, and other elements; Sigma Aldrich) and a  ${}^7\text{Li}$ -rich sample (the isotopic composition of the 99.9% pure natural lithium ( ${}^7\text{Li}$ ) was 92.41% atomic  ${}^7\text{Li}$  and 7.59% atomic  ${}^6\text{Li}$ ; the impurity composition was the same as in the case of the  ${}^6\text{Li}$ ; Sigma Aldrich), which we refer to as  ${}^6\text{Li}$  and  ${}^7\text{Li}$  samples respectively in the rest of this manuscript.

All measurements were carried out in a DAC using electrical resistance as a means of determining the superconducting transition temperatures. All pressure increases were carried out at room temperature. This return to room temperature after every measurement allowed the samples to be transformed to their equilibrium phase. Lithium reacts readily with many materials including diamond<sup>20, 22, 30</sup>, which may cause a DAC to fail. In order to prevent any such reactions, compressed, dehydrated alumina powder was used both as an electrical insulator and a pressure medium<sup>31</sup>. This allowed us to keep the samples at room temperature inside the DAC without risking failure of the diamonds. An insulated gasket was made from a 250  $\mu\text{m}$  thick stainless-steel foil, pre-indented to a thickness of 40-55  $\mu\text{m}$ . Two pressure chambers with initial diameters of 110  $\mu\text{m}$  were symmetrically drilled 10-20  $\mu\text{m}$  apart from each other on the gasket and several ruby spheres were dispersed evenly in each pressure chamber. The gasket then was insulated with a mixture of epoxy and alumina. Pure alumina,

which was heat treated at 110°C to remove moisture, was used as the pressure transmitting medium inside the sample chambers. While alumina is a non-hydrostatic pressure medium, the maximum pressure gradient remained below  $\pm 0.8$  GPa up to the highest pressure measured ( $\sim 26$  GPa). An isolated quasi-four probe arrangement was built on each sample chamber using platinum electrodes. To eliminate the interference between the two circuits, each circuit was connected to a separate lock-in amplifier and run on a different frequency ( $\sim 5$  and 13 Hz). To prevent any possible chemical reactions, the samples were loaded and pressurized inside a high purity argon glovebox. An AC current of  $I_{\text{rms}} \sim 100 \mu\text{A}$  was applied across each sample. Since the arrangement used here was a quasi four probe, a small portion of the signal always came from the piece of Pt electrode in the path. The onset of superconductivity was defined by the temperature at which the resistance of sample drops to zero (fig. 2a). As an additional test of superconductivity, we used a small magnetic field ( $\sim 100$  Oe) to suppress  $T_c$  (fig. 2b and 2c). Fig. 3a shows the superconducting phase diagram of  ${}^6\text{Li}$  and  ${}^7\text{Li}$  for pressures between 16 and 26 GPa. These measurements for  ${}^7\text{Li}$  are consistent with the initial trends of previously reported results by Deemyad & Schilling. These results, for comparison, are plotted together with all measurements of  ${}^7\text{Li}$  in figure 3. The sign of  $\left(\frac{dT_c}{dP}\right)$  in the pressure range  $16\text{GPa} < P < 26\text{GPa}$  changes two times for  ${}^6\text{Li}$ . In this region, the slope is always positive, though not constant, for  ${}^7\text{Li}$ . A change in slope may be indicative of the presence of a structural phase boundary (hR9 to fcc for  ${}^7\text{Li}$ ). Between 16 and 21.5 GPa, the superconducting  $T_c$  of  ${}^6\text{Li}$  is higher than that of  ${}^7\text{Li}$ . Figure 3c shows the calculated values of the isotopic coefficient,  $\alpha$ , as a function of pressure. The lowest pressure points at 16 and 18 GPa for  ${}^6\text{Li}$  display an initial positive slope  $\left(\frac{dT_c}{dP}\right)$ , however, the paucity of data in this region makes assigning a slope for the  $\alpha$  value impossible. For  $18\text{GPa} < P < 21.5\text{GPa}$ , the value of the isotopic coefficient decreases monotonically with pressure, and the value of  $\alpha$  is always higher than expected for BCS-type superconductors,  $1 \lesssim \alpha \lesssim 4$ . This large departure from BCS-type behavior may be explained if the two isotopes have different structures in this pressure range. For  $P > 21.5\text{GPa}$ , the value of the isotopic coefficient,  $\alpha$ , changes sign and remains constant within error ( $\alpha \approx -1.5 \pm 0.5$ ).

The structures of Li as a function of pressure (for pressures above 0.65 GPa<sup>32</sup>) are not known for  $T < 77$  K, which contains the boundaries of the martensitic phase<sup>30</sup>. This phase is thought to play an important role in superconductivity. Moreover, the isotopic dependence of the structures of lithium is not known at all in this pressure regime. Between 16-22 GPa,  ${}^6\text{Li}$  exhibits a change from a positive to a negative slope in  $T_c$ . In contrast,  ${}^7\text{Li}$  shows a positive slope in the entire range where superconductivity was observed. It is possible that the large difference in  $T_c$ 's, the initial change in slope for  ${}^6\text{Li}$ , and the opposite slopes observed between 18-22 GPa are caused by a low temperature structure in  ${}^6\text{Li}$  not present in  ${}^7\text{Li}$ . Low temperature structural studies are required to characterize this region. Above 21.5 GPa, the superconducting  $T_c$  of  ${}^6\text{Li}$

falls below that of  ${}^7\text{Li}$ , this effect remains until the highest pressure studied here,  $\sim 26$  GPa. The inverse isotope effect in conventional superconducting systems is noted in some transition metal hydrides (MH), such as PdH, and in the element  $\alpha\text{-U}$ <sup>33-36</sup>. The inverse isotope effect in MH has been attributed to the existence of large quantum effects in hydrogen, which cause anharmonicity in phonon spectra<sup>37,38</sup>; an explanation which cannot account for the behavior of  $\alpha\text{-U}$ . If the unusual isotope effect in Li is solely a consequence of its zero point displacements and a consequent anharmonicity in its lattice, Li is the only elemental solid known to exhibit such behavior. However, in the present case the electronic and structural effects may be entangled.

It is also notable that isotopes of Li possess different quantum statistics, and natural lithium has been shown to exhibit nuclear order at one atmosphere<sup>39</sup>. The magnetic order in lithium isotopes under pressure may also contribute to their unusual superconducting isotope effects.

In summary, we studied the superconductivity of isotopically enriched  ${}^6\text{Li}$  in comparison to the superconductivity of natural lithium. We observed the following differences between the superconducting properties of the two samples: a) In the pressure range of this study,  ${}^6\text{Li}$  shows two changes of the sign of the slope of  $\left(\frac{dT_c}{dP}\right)$  from positive to negative at  $\sim 18$  GPa, then to positive again at  $\sim 22$  GPa, while the superconducting  $T_c$  of  ${}^7\text{Li}$  monotonically increases with pressure, though the slope increases above 21.5 GPa. The change of the sign of the slope  $\left(\frac{dT_c}{dP}\right)$  for  ${}^6\text{Li}$  suggests differences in the high pressure structures of the two isotopes and possibly the existence of additional structures in  ${}^6\text{Li}$  that do not occur in  ${}^7\text{Li}$ . b) Below 21.5 GPa, a direct superconducting isotope effect ( $\alpha > 0$ ) is observed with  $1 < \alpha < 4$ . Above 21.5 GPa, an inverse superconducting isotope effect is observed with  $-2 < \alpha < -1$ . The deviation of the superconducting isotope effects in lithium from conventional BCS-type superconductivity under pressure suggests both the presence of quantum solid behavior and its enhancement under compression. Observation of this quantum solid behavior is enhanced in the temperature region in which thermal energy is not dominant. Studies on low temperature structures and magnetism of lithium isotopes at these densities are necessary to provide a complete picture of its quantum solid behavior. They may guide further investigations of quantum solidity in metallic hydrogen.

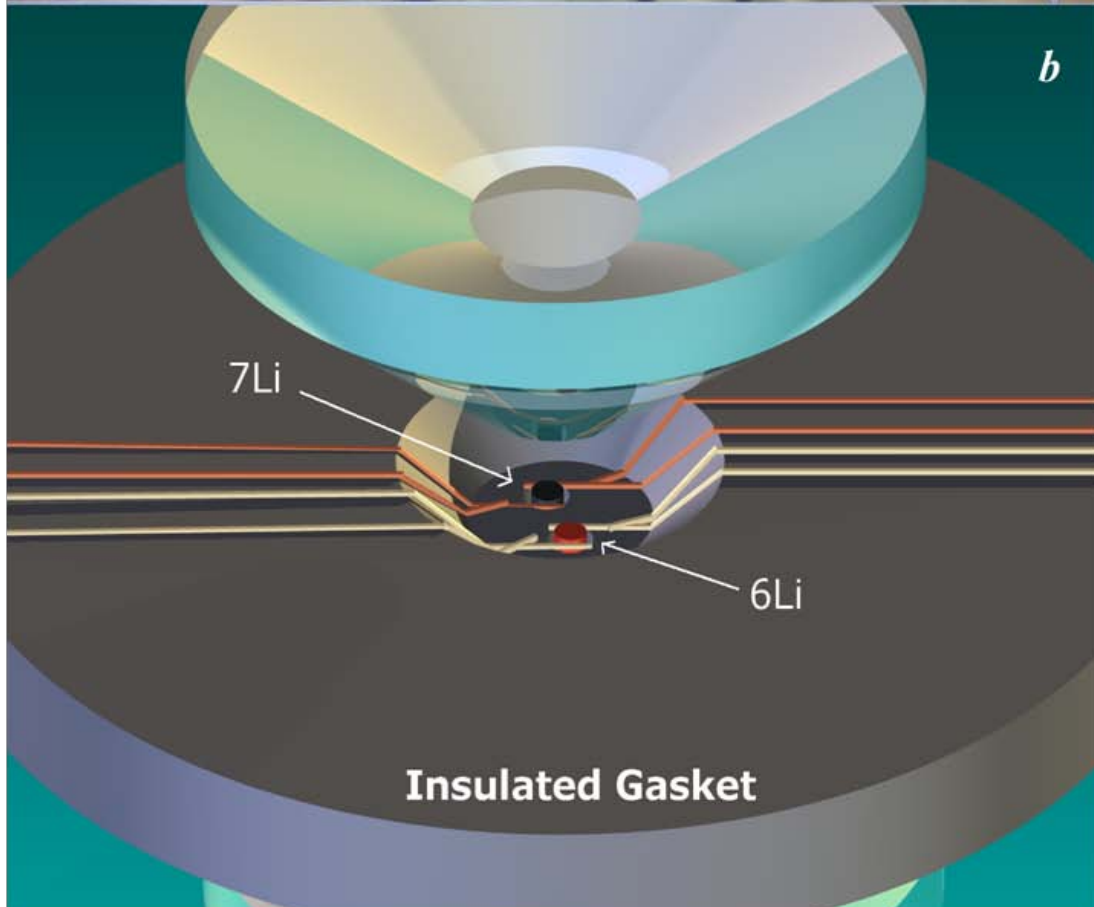
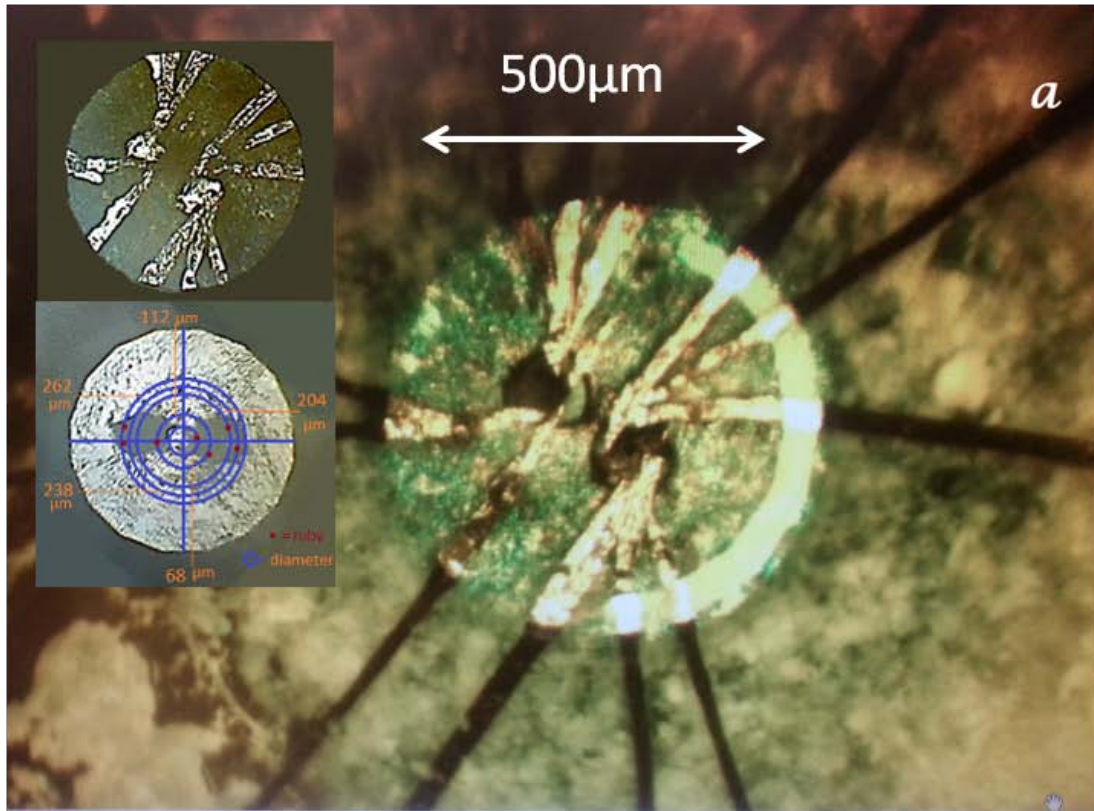


Fig. 1) a) Twin chamber gasket built on a 500  $\mu\text{m}$  culet diamond which is used in the present experiments in a DAC for simultaneous measurements of superconductivity. Each pressure chamber has a pair of extra Pt leads and contains several pieces of ruby for accurate determination of pressure gradient within each pressure chamber. The insets show the gasket and samples under reflected light only, at 21.3 GPa, demonstrating the metallic appearance of both samples and map of ruby pieces inside each pressure chamber in the same run . b) Schematic drawing of the twin chamber design used in the experiments. Small portions of the platinum leads in the path contribute to the total resistance measured for each sample. The electrodes for measuring the resistance of  $^6\text{Li}$  and  $^7\text{Li}$  are shown in different colors.

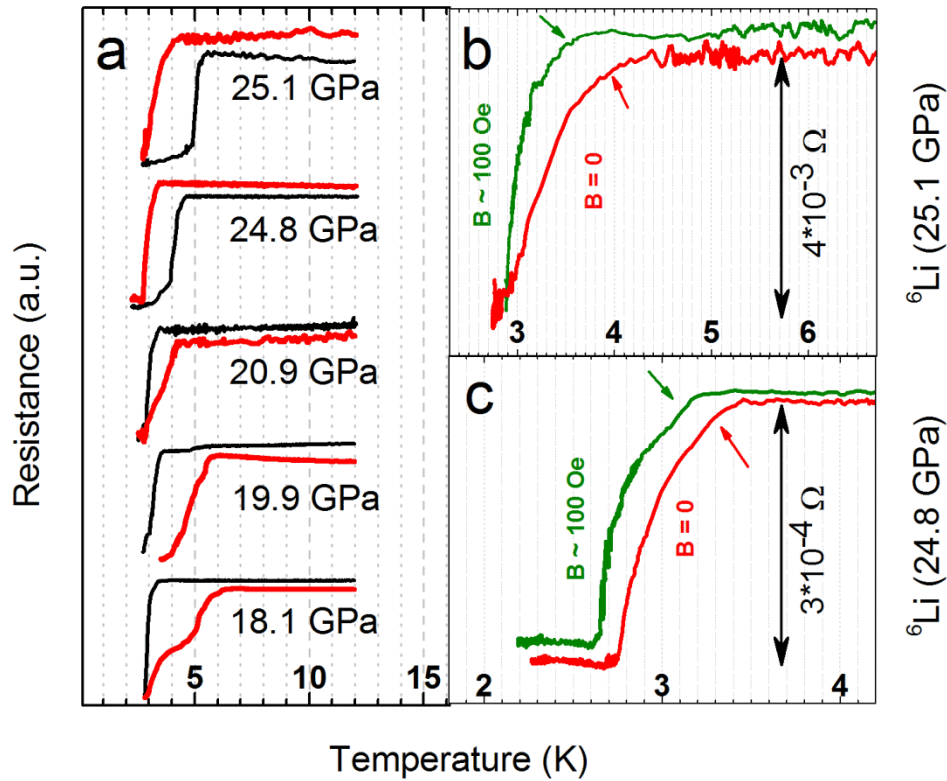


Fig. 2) a) Superconducting transitions as determined by electrical resistivity. All black lines show transitions for  ${}^7\text{Li}$ , red lines are the transitions for  ${}^6\text{Li}$ . Each pair shows the simultaneous measurement. The double step in 18.1 GPa transition of  ${}^6\text{Li}$  may be related to presence of mixed phases with different  $T_c$ 's at a structural phase boundary. The samples' resistances in a normal state above their superconducting transitions is  $\sim 0.5\text{--}10\text{ m}\Omega$  varying by the sample size and geometry. These values would give an estimate of  $\rho \approx 0.5 - 1 \mu\Omega \cdot \text{cm}$ , at room temperature, for a typical sample size of  $50 \times 50 \times 10 \mu\text{m}^3$ . An RRR value of  $\sim 75$  is estimated from ambient pressure measurements on the samples used here<sup>40</sup>. The transitions above are scaled for ease of comparison. b,c) The shift of  $T_c$  with an applied external magnetic field of  $B \sim 100$  Oe for  ${}^6\text{Li}$  at 23.3 and 26.6 GPa.  $B \sim 100$  Oe for green lines and  $B = 0$  for red lines.

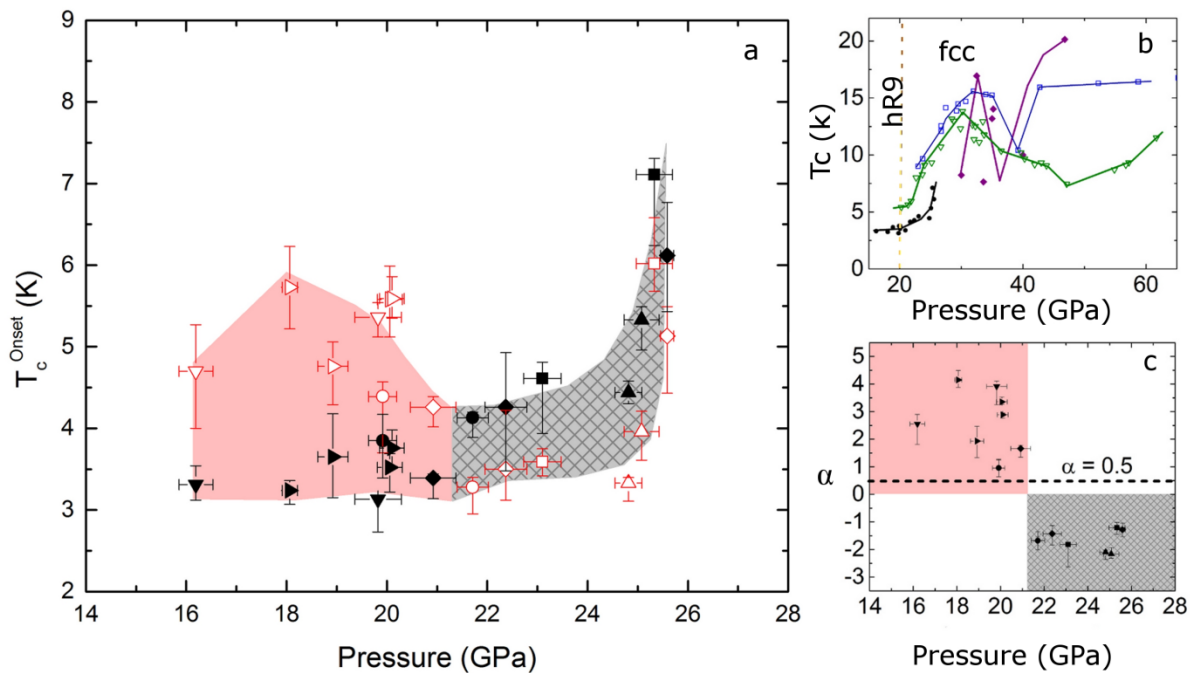


Fig. 3) a) Superconducting phase diagram of lithium isotopes. Open shapes represent  ${}^6\text{Li}$ , solid shapes represent  ${}^7\text{Li}$ . The different shapes designate separate loadings. The pink shaded region from 18 GPa to 21.5 GPa shows the direct isotope effect with a large difference in the  $T_c$ 's for  ${}^6\text{Li}$  and  ${}^7\text{Li}$ . The grey shaded region shows the inverse isotope effect from 21.5 GPa to 26 GPa. b) Comparison of the various superconducting phase diagram of natural lithium measured by various techniques (Open triangles: Deemayd and Schilling, Open squares: Struzhkin et al., diamonds: Shimizu et al. and circles: This study). The solid lines are guide to eye. Dashed line is the speculated boundary between hR9 and fcc at low temperature. c) The isotope coefficient,  $\alpha$ , as a function of pressure. The dashed line at  $\alpha = 0.5$  shows the expected value for a conventional isotope effect.

### Acknowledgments:

The authors would like to thank Prof. N. W. Ashcroft for insightful discussions on high pressure properties of quantum solids and critically reviewing this manuscript. Authors are grateful for experimental assistance from R. McLaughlin, D. Sun, H. Malissa and Z. Jiang. This work is supported by NSF-DMR grant # 1351986. JKB acknowledges the financial support from the University of Utah UROP fund.

## References:

1. A. M. J. Schaeffer and S. Deemyad, review of scientific instruments **84** (9), 095108 (2013).
2. B. Shukla, N. V. C. Shekar, N. R. S. Kumar, T. R. Ravindran, P. Sahoo, S. Dhara and P. C. Sahu, Journal of Physics: Conference Series **377** (1), 012014 (2012).
3. N. W. Ashcroft, Physical Review Letters **21** (26), 1748-1749 (1968).
4. E. G. Brovman, Y. Kagan and A. Kholas, Sov. Phys. JETP **35**, 783-792 (1972).
5. E. Babaev, A. Sudbo and N. W. Ashcroft, Nature **431** (7009), 666-668 (2004).
6. S. A. Bonev, E. Schwegler, T. Ogitsu and G. Galli, Nature **431** (7009), 669-672 (2004).
7. T. W. Barbee, A. Garcia and M. L. Cohen, Nature **340** (6232), 369-371 (1989).
8. N. W. Ashcroft, Nature **340** (6232), 345-346 (1989).
9. M. I. Eremets and I. A. Troyan, Nat Mater **10** (12), 927-931 (2011).
10. N. W. Ashcroft, Physical Review B **39** (15), 10552-10559 (1989).
11. R. J. Hemley, C. S. Zha, A. P. Jephcoat, H. K. Mao, L. W. Finger and D. E. Cox, Physical Review B **39** (16), 11820-11827 (1989).
12. S. Stishov, Physics-Uspekhi **44** (3), 285-290 (2001).
13. C. F. Richardson and N. W. Ashcroft, Physical Review B **55** (22), 15130-15145 (1997).
14. J. Tuoriniemi, K. Juntunen-Nurmilaukas, J. Uusvuori, E. Pentti, A. Salmela and A. Sebedash, Nature **447** (7141), 187-189 (2007).
15. D. Kasinathan, J. Kuneš, A. Lazicki, H. Rosner, C. S. Yoo, R. T. Scalettar and W. E. Pickett, Physical Review Letters **96** (4), 047004 (2006).
16. N. E. Christensen and D. L. Novikov, Physical Review Letters **86** (9), 1861-1864 (2001).
17. T. Bazhiron, J. Noffsinger and M. L. Cohen, Physical Review B **84** (12), 125122 (2011).
18. E. L. Gromnitskaya, O. V. Stal'gorova and S. M. Stishov, JETP Letters **69** (1), 38-43 (1999).
19. A. F. Goncharov, V. V. Struzhkin, H.-k. Mao and R. J. Hemley, Physical Review B **71** (18), 184114 (2005).
20. K. Shimizu, H. Ishikawa, D. Takao, T. Yagi and K. Amaya, Nature **419** (6907), 597-599 (2002).
21. S. Deemyad and J. S. Schilling, Physical Review Letters **91** (16), 167001 (2003).
22. V. V. Struzhkin, M. I. Eremets, W. Gan, H.-k. Mao and R. J. Hemley, science **298** (5596), 1213-1215 (2002).
23. E. E. Treyeva and T. I. Trapezina, Physics Letters **37A** (1), 83-84 (1971).
24. D. Stroud and N. W. Ashcroft, Physical Review B **5** (2), 371 (1972).
25. C. Friedli and N. W. Ashcroft, Physical Review B **12** (12), 5552 (1975).
26. A. Ubbelohde, Transactions of the Faraday Society **32**, 525-529 (1936).
27. V. Kogan, Physics-Uspekhi **5** (6), 951-975 (1963).
28. J. Dugdale, D. Guban and K. Okumura, Proceedings of the Royal Society of London. Series A. Mathematical and Physical Sciences **263** (1314), 407-419 (1961).
29. A. W. McReynolds, Journal of Applied Physics **20** (10), 896-907 (1949).
30. C. L. Guillaume, E. Gregoryanz, O. Degtyareva, M. I. McMahon, M. Hanfland, S. Evans, M. Guthrie, S. V. Sinogeikin and H. K. Mao, Nat Phys **7** (3), 211-214 (2011).
31. A. M. J. Schaeffer, W. B. Talmadge, S. R. Temple and S. Deemyad, Physical Review Letters **109** (18), 185702 (2012).

32. H. G. Smith, R. Berliner, J. D. Jorgensen, M. Nielsen and J. Trivisonno, *Physical Review B* **41** (2), 1231-1234 (1990).
33. H. Hemmes, A. Driessen, R. Griessen and M. Gupta, *Physical Review B* **39** (7), 4110-4118 (1989).
34. R. D. Fowler, J. D. G. Lindsay, R. W. White, H. H. Hill and B. T. Matthias, *Physical Review Letters* **19** (16), 892-895 (1967).
35. J. Fan and Y. Malozovsky, *International Journal of Modern Physics B* **17** (18n20), 3458-3464 (2003).
36. T. Skoskiewicz, A. Szafranski, W. Bujnowski and B. Baranowski, *Journal of Physics C: Solid State Physics* **7** (15), 2670 (1974).
37. A. Karakozov and E. Maksimov, *Zh. Eksp. Teor. Fiz* **74**, 681 (1978).
38. I. Errea, M. Calandra and F. Mauri, *Physical Review Letters* **111** (17), 177002 (2013).
39. K. Juntunen and J. Tuoriniemi, *Physical Review Letters* **93** (15), 157201 (2004).
40. T. Matsuoka and K. Shimizu, *Nature* **458** (7235), 186-189 (2009).